Available online at www.sciencedirect.com

ScienceDirect

Procedia Earth and Planetary Science 11 (2015) 180 – 188

Procedia Earth and Planetary Science

Global Challenges, Policy Framework & Sustainable Development for Mining of Mineral and Fossil Energy Resources (GCPF2015)

Lithological Discrimination and Mapping using ASTER SWIR Data in the Udaipur area of Rajasthan, India

Chandan Kumar[a,*], Amba Shetty[a], Simit Raval[b], Richa Sharma[c], P.K. Champati Ray[c]

[a]*Department of Applied Mechanics & Hydraulics, National Institute of Technology Karnataka, Mangalore 575025, India*
[b]*School of Mining Engineering, University of New South Wales, Sydney NSW 2052, Australia*
[c]*Department of Geosciences & Geohazards, Indian Institute of Remote Senisng, Indian Space Research Organization, Dehradun 248001, India*

Abstract

The present study applies the Principal Component Analysis (PCA), Minimum Noise Fraction (MNF) and Independent Component Analysis (ICA) transformation on calibrated (orthorectified, cross-track illumination and atmospherically corrected) Advanced Spaceborne Thermal Emission and Reflection Radiometer (ASTER) Shortwave Infrared (SWIR) data in the hostile terrain of Udaipur area. The area has continuous geological sequences, various rock types and economic deposits of lead and zinc, copper, micas and marbles. The proposed Band Combination (BC) derived from PCA (R: PC2, G: PC1, B: PC3), MNF (R: MNF2, G: MNF1, B: MNF3) and ICA (R: IC2, G: IC3, B: IC1) has shown its effectiveness in lithological mapping. The BC derived from ICA shows a great success over BC of PCA and MNF transform to discriminate various lithological units. The lithological map derived from BC of ICA transform shows strong agreement with the published lithology map and field investigation. Therefore, ASTER SWIR data coupled with less explored advanced image enhancement technique like ICA are recommended as a rapid and cost effective tool for lithological discrimination and mapping.

Peer-review under responsibility of organizing committee of the Global Challenges, Policy Framework & Sustainable Development for Mining of Mineral and Fossil Energy Resources.

Keywords: ASTER; Band Combination; Independent Component Analysis; Lithological Mapping; Minimum Noise Fraction; Principal Component Analysis

1. Introduction

The utility of remotely sensed data in geological applications such as lithological discrimination, mineral detection, mineral potential and hydrothermal alteration mapping at various scales have shown a great success[5,17,24, 26,27,29]. Spaceborne multispectral sensors, particularly Landsat Thematic Mapper (TM)

* Corresponding author. Tel.: +918147299523.
E-mail address: chandankumar138@gmail.com

Peer-review under responsibility of organizing committee of the Global Challenges, Policy Framework & Sustainable Development for Mining of Mineral and Fossil Energy Resources.
doi:10.1016/j.proeps.2015.06.022

and Enhanced Thematic Mapper (ETM+) launched in 1982 and 1999 with 5 and 8 spectral channels respectively have been well employed for such applications[6,26]. However, the launch of the Advanced Spaceborne Thermal Emission Reflection Radiometer (ASTER) in December 1999 with three spectral bands in the Visible/near Infrared (VNIR) region, six spectral bands in the Shortwave Infrared (SWIR) region and five spectral bands in the Thermal Infrared (TIR) region with 15m, 30m and 90m spatial resolution has provided a new prospective of investigating earth's surface material for various applications[5,7,21,27]. The enhanced resolutions, high Signal to Noise Ratio (SNR), the effective spectral coverage and global data availability makes ASTER more suitable particularly for operational geological applications. The three subsystems of ASTER sensor, i.e. VNIR, SWIR and TIR has different roles to play in spectroscopy for geological applications such as the VNIR region provides spectral features of transition metals such as iron, SWIR region is very effective for analyzing spectral characteristics of carbonate, hydrate and hydroxide minerals, and TIR region is effective for characterization of silicates[3, 7]. The ASTER sensor acquires earth's surface imagery in the VNIR, SWIR and TIR wavelength regions and has offered a great opportunity of using these datasets for mapping of various lithological units[1,7,26], minerals[5], hydrothermal alteration such as propylitic, argillic, phyllic and potassic zone[4,15,16,19]. Various image enhancement techniques such as Principle Component Analysis (PCA), Minimum Noise Fraction (MNF), Band Ratios (BRs), Band Combinations (BCs) and Spectral Indices (SIs) [6,7,18,19,27]; spectral mapping algorithms such as Spectral Angle Mapper (SAM), Spectral Feature Fitting (SFF), Matched Filter (MF), Constrained Energy Minimization (CEM), Linear Spectral Unmixing (LSU), Mixture Tuned Matched Filter (MTMF) have been well employed on ASTER datasets to obtain the lithological, mineral and hydrothermal alteration maps with reasonable accuracies[5,8,12,15-17,28]. Most of the full and sub-pixel spectral algorithms require target spectra or endmember to detect and classify them, which needs a rigorous procedure of spectral data extraction either from image, laboratory or spectral library[14]. In this study, discussion is restricted to PCA, MNF and ICA derived BCs, which further implemented on ASTER SWIR data to discriminate the various lithological units. Most of the previous studies on lithological mapping using ASTER data are carried out by employing PCA, MNF and BRs derived BCs. To the best of our knowledge rare publication available as per as the utility of ICA for lithological mapping is concerned. The area under investigation consist of various economic deposits (such as lead and Zinc, copper, micas, barytes and marbles) and hydrothermal alteration, which has not been investigated using ASTER data. Therefore, the objective of the present study is to demonstrate the utility of less explored ICA on ASTER SWIR data for lithological discrimination and mapping in the Udaipur area, Rajasthan.

2. Location and geological setting of the study area

The study area (Fig. 1) of arid to semiarid climate is situated in the south eastern part of Rajasthan (India), which comprises a continuous geological sequences and various rock types (Fig. 1b) from oldest Archean to recent alluvium formations. It has occurred during three orogenic cycles represented by terrains named Banded Gneissic Complex (BGC), Aravalli Super Group (ASG) and Delhi Super Group (DSG)[23]. The BGC in Rajasthan can be dived into three major rock groups as Mangalwar Complex (MC), Sandmata Complex (SC) and Hindoli Group (HG)[10]. The MC dominantly consist of heterogeneous assemblage of amphibolite-facies metamorphites comprising of migmatites, composite gneisses, feldspathic mica schist, sillimanite-kyanite, mica schist, hornblende schist, granite gneiss and amphibolite along with minor carbonates[10]. The BGC is overlain by the ASG, which can be divided into two principal facies sequences i.e. the self facies in the East comprising mafic, volcanics, coarse clastics and carbonates, and carbonate free deep sea facies in the West containing dominantly phyllites with the quartzite bands[22]. The shelf facies is further subdivided into volcanic dominated Delwara group and the volcanic free Debari group[25]. The Delwara group occupies the lowermost sequence in the ASG and mainly comprises of mafic volcanic, clean-washed quartzite, quartz pebble conglomerate and banded iron formation, whereas the Debari group constituent the middle ASG and consist of coarse clastics, carbonates and phyllites[25]. The litho-sequence comprising greywacke and phyllite is designated as the Udaipur formation, which is overlain by a carbonate sequence hosting Pb-Zn mineralization of Zawar formation[25].

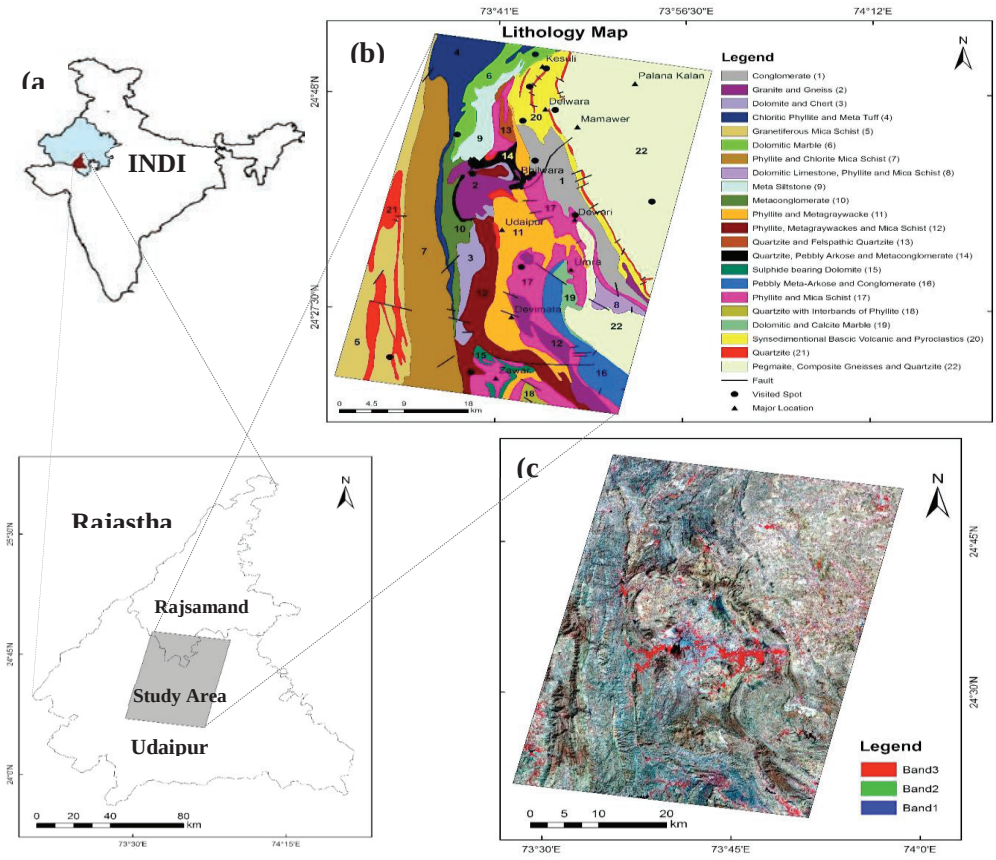

Fig. 1. The location and geology setting of the study area. (a) Location Map; (b) Lithological Map (prepared after GSI 1982) with Visited Spot and Major Locations; (c) The False Colour Composite (FCC) Map prepared from ASTER VNIR Image (R: band3, G: band2, B: band1) shows the topography and land cover class.

The carbonate free and pelites dominant sequence arenite bands of ASG is named as Jharol group and mainly composed of phyllites, chlorite schist, garnetiferous mica schist[10,23]. The area has gone under a high degree of metamorphism and the major lineaments trend shows NE-SW and E-W direction. These rocks exhibit various folding and hydrothermal alteration, which could be further linked with identification of new economic deposits in the area. The major lithological units found in the study area are conglomerate, granite, gneiss, phyllite, mica schist, dolomite, quartzite, volcanics and pegmatites, etc. shown in the Fig. 1b.

3. Satellite image and collateral datasets

A cloud free Level 1B (geometric and radiometric corrected) ASTER data of the month March 2004 was obtained from Earth Remote Sensing Data Analysis Centre (ERSDAC) Japan for the study. The data consist of 3 VNIR, 6 SWIR and 5 TIR spectral bands. In this study, six spectral bands of the SWIR region were selected for the processing. The detailed specification of the ASTER sensor is given in Table 1. Collateral datasets such as the Geological Survey of India (GSI) district resource map (1:250000 scale) and published literature of the Udaipur and Rajsamand districts of Rajasthan was used as a geological guide to interpret and assess the image results. Due to the challenging topography and hostile conditions of the study area only few spots were visited to verify the image derived lithological map. In this study, ENVI® 4.8 and ArcGIS® 9.3 software packages was used to process the ASTER imagery and preparation of GIS layers respectively.

Table 1. ASTER sensor specification (Gomez et. al [9])

Characteristics	VNIR		SWIR		TIR	
Spectral coverage	Band 1	0.52-0.60 µm	Band 4	1.6-1.7 µm	Band 10 µm	8.125-8.475
	Band 2	0.63-0.69 µm	Band 5	2.145-2.185 µm	Band 11 µm	8.475-8.825
	Band 3N	0.76-0.86 µm	Band 6	2.185-2.225 µm	Band 12 µm	8.925-9.275
	Band 3B	0.76-0.86 µm	Band 7	2.235-2.285 µm	Band 13 µm	10.25-10.95
	(N: Nadir looking)		Band 8	2.295- 2.365 µm	Band 14 µm	10.95-11.65
	(B: Backward looking)		Band 9	2.36-2.43 µm		
Spatial resolution (m)	15		30			
Swath width (km)	60		60			
Signal quantization level (bits)	8		8		90	
					60	
					12	

4. ASTER image processing and analysis

4.1. ASTER image pre-processing

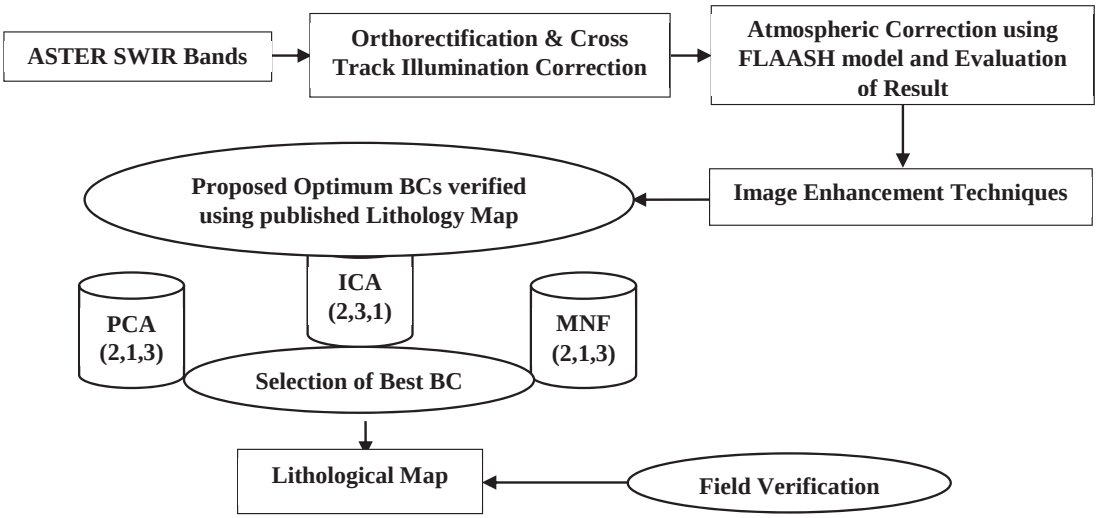

Fig. 2. The flow chart of adopted methodology for lithological discrimination and mapping

The spatial subset of 2448 km^2 Level1B radiance at sensor ASTER SWIR spectral bands has gone under orthorectification by projecting the raw image to the Universe Transvers Macerator (UTM) 43 zone and True North, followed by cross track illumination correction to remove the effects of energy overspill from band 4 into bands 5 and 9. The SWIR bands should be corrected for cross track illumination effects before any further processing for better and accurate results[11]. Subsequently, these bands were subjected to atmospheric correction using Fast Line of Sight Atmospheric Analysis Spectral Hypercubes (FLAASH) model of the ENVI® 4.8 software, which incorporates MODTRAN® radiation transfer code to remove the atmospheric attenuations to produce reflectance imagery in a such a way that a spectral curve from each pixel of multispectral image can be derived for target detection, discrimination and classification[14]. The FLAASH model needs various parameters to convert raw image to reflectance image, which was derived from the metadata of the original image. The ASTER Digital Elevation Model

(DEM) of 30 m spatial resolution of the area has been used to derive average elevation of the terrain and then the elevation value was used in the FLAASH. To evaluate the atmospheric correction result two basic features of the earth's surfaces such as vegetation (appeared in red colour on the FCC) and limestone/calcite (commonly appeared as white or bright tone), which shows distinct spectral signature was used to evaluate the result of FLAASH model by comparing their image and ASTER band pass resampled library spectra of the Jet Propulsion Library (JPL) available in ENVI® 4.8. After preprocessing of ASTER image it has been further subjected to image noise reduction and enhancement techniques such as PCA, MNF and ICA Transform. The detailed flow chart of the methodology adopted in ASTER image processing and analysis for lithological discrimination and mapping is shown in Fig. 2.

4.2. ASTER image enhancement and analysis

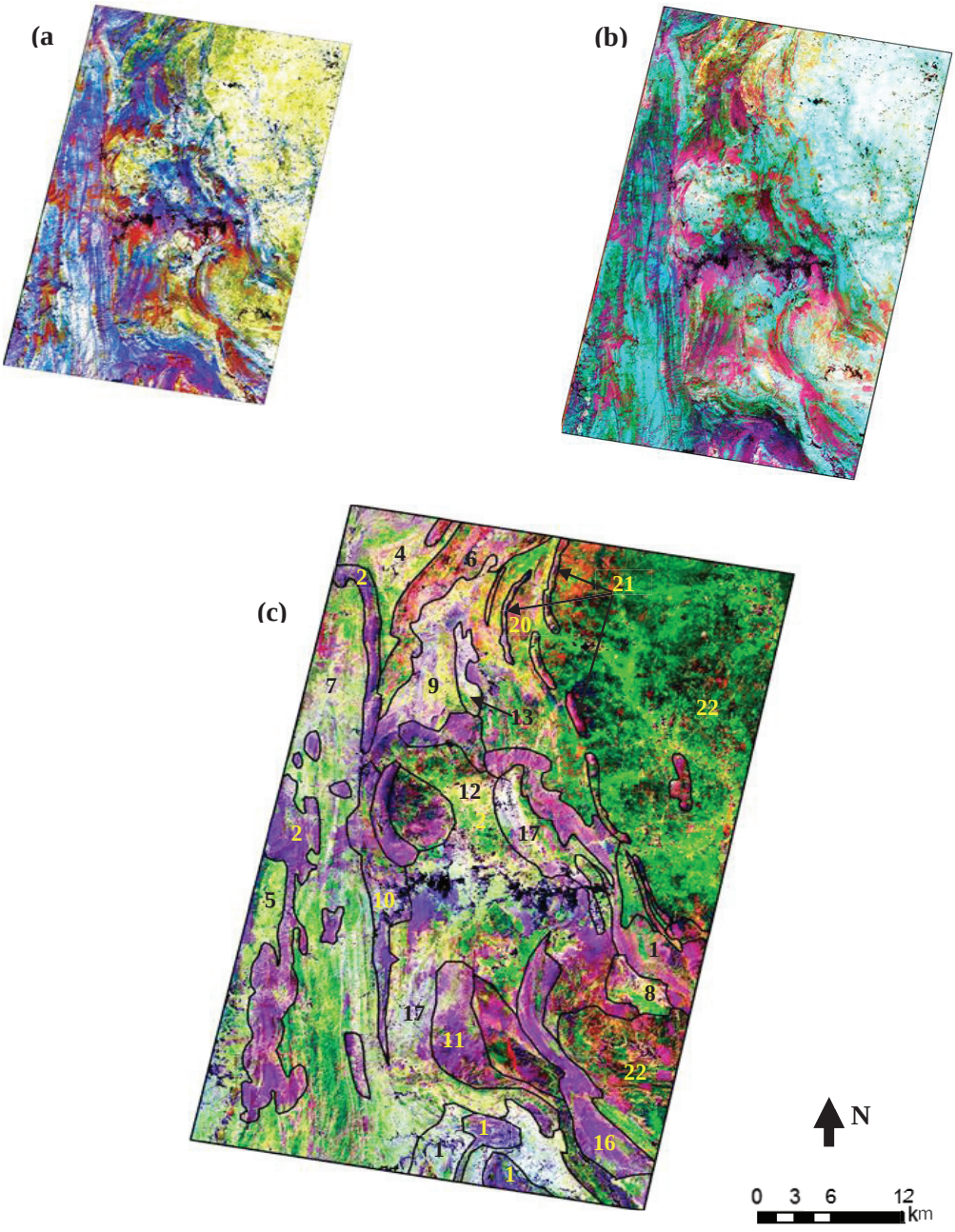

Fig. 3. Proposed BCs derived from PCA, MNF and ICA Transform for Lithological Discrimination and Mapping. (a) BC derived from PCA (R: PC2, G: PC1, B: PC3); (b) BC derived from MNF (R: MNF2, G: MNF1, B: MNF3); and (c) BC derived from ICA (R: IC2, G: IC3, IC1) shows major Lithological Units (refer Fig. 1b for the legend of lithological units). Masked region (vegetation and water bodies) is shown in black colour.

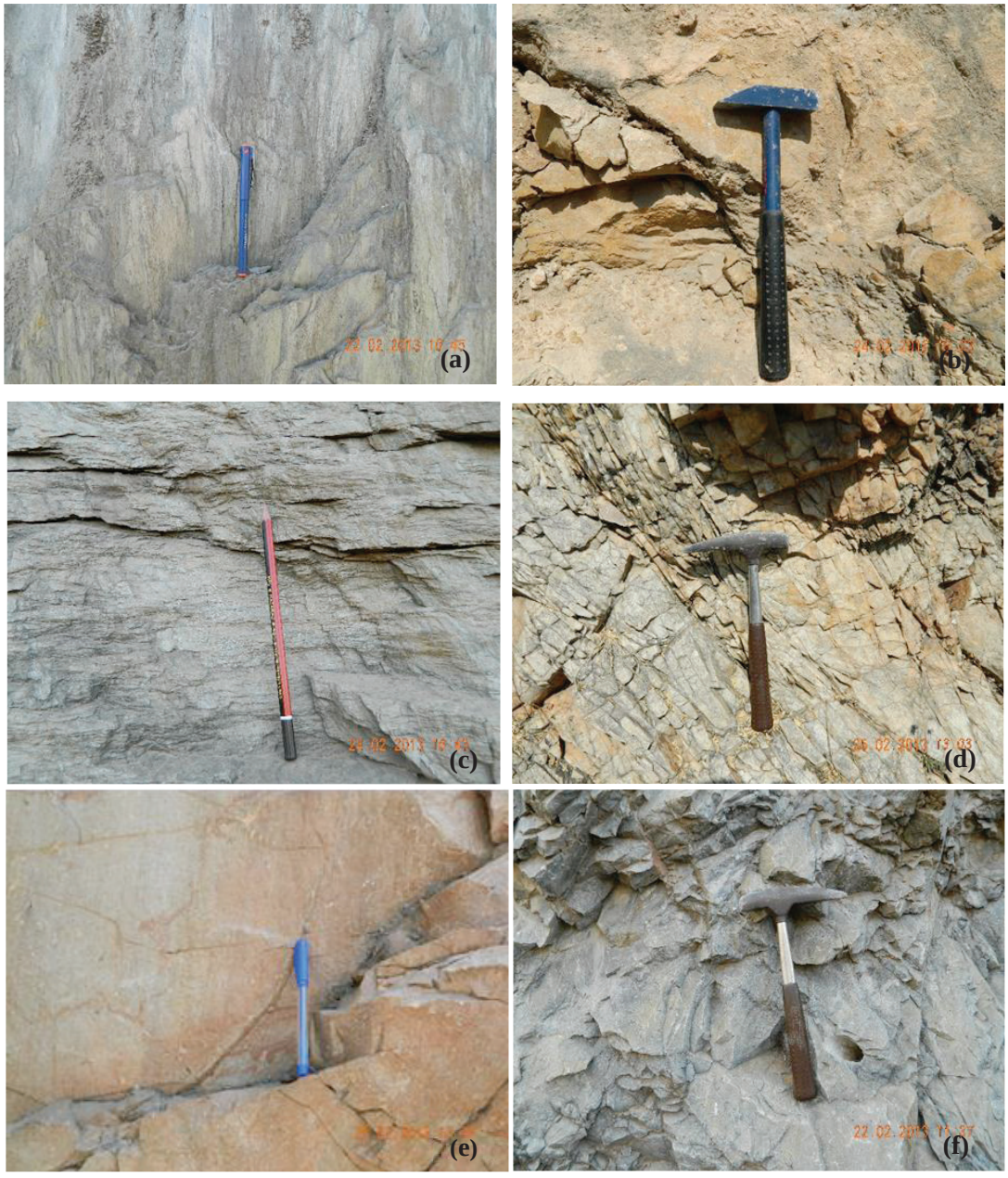

Fig. 4. The Field Photographs of the study area during Field Investigation. (a). Phyllite with Mica Schist; (b). Weathered Conglomerate with volcanic tuffs; (c) Mica Schist; (d). Highly fractured Quartzite; (e). Ferruginous Quartzite; (f). Dolomitic Stone/Marble in mining area. Photographs were taken by looking straight to the exposures.

Image enhancement techniques such as PCA, MNF and ICA transform have been implemented on the calibrated SWIR spectral bands of the ASTER image. These image enhancement techniques are also called as spectral data reduction as they reduce the spectral redundancy of the image. The PCA transform is a multivariate statistical technique and used to produce uncorrelated output bands, to segregate noise components and to reduce the spectral dimensionality of the data in a such a way that first PC band contains a high variance or eigen value, the second PC band contains second high variance and the last

PC band contains the minimum variance, high correlation and noise[20,29] and hence PCA transform helps to enhance and separate spectral signatures from the background[5]. The MNF is the enhanced version of the PCA, which consist of two cascaded PCA rotations. The first PC rotation performs noise whitening and resulting in transformed data in which the noise has unit variance and no band to band correlation whereas the second rotation uses PCs derived from the original image data after they have been noise-whitened by first rotation and rescaled by the noise standard deviation. Similar to PCA output bands the first MNF band contains of high variance, the second MNF band contains the second high variance, but the last MNF band is highly correlated and noisy[17].

The MNF transform has been extensively used in multispectral and hyperspectral data for feature extraction, noise whitening and spectral data reduction. The PCA and MNF transform have been extensively used in the lithological and alteration mapping[15,16,18,19,21]. Both PCA and MNF transform are based on second order statistics whereas ICA transform uses higher order statistics for the signal separation and feature extraction. The ICA could reveal more spectral information as compared to PCA and MNF[13] and which could further enhance the image for better lithological discrimination. The key benefit of ICA includes the extraction of feature even it covers a small fraction in pixels[13]. Similar to both PCA and MNF output bands the first IC band contains of high variance, the second IC band contains second high variance and the last IC band contains minimum variance, high correlation and noise. After computing PCA, MNF and ICA transform various BCs were tested and evaluated with a published lithology map to select an optimum BC for each transformation to discriminate the lithological units in the area. The optimum BCs derived from PCA (R: PC2, G: PC1, B: PC3), MNF (R: MNF2, G: MNF1, B: MNF3) and ICA (R: IC2, G: IC3, B: IC1) is shown in the Fig. 3a, 3b and 3c respectively, exhibits different levels of lithological discrimination. After preparing BCs masking of vegetation and water bodies was carried out using the Normalized Difference Vegetation Index (NDVI) and ASTER band 4 respectively.

The proposed BC derived from PCA is easily able to discriminate pegmatites, phyllite and schist, but fails to discriminate various rock types such as conglomerate, quartzite ridges, synsedimentional volcanic and pyroclastic whereas the proposed BC derived from MNF is almost able to discriminate these rock types but fails to specify a distinct lithological boundary for discrimination and mapping.

The proposed BC derived from ICA shows an enhanced perspective and each lithological unit were easily identified, discriminated as well as able to specify the distinct boundary between them. It is also important to mention here that BC derived from ICA also offers to identify small outcrops, which was not well distinguish in PCA and MNF BCs. The lithological map derived from ICA BC of ASTER SWIR was further verified with published GSI district resource map of the area. A field verification (Fig. 4) of the few sites in the area was also carried to evaluate the image derived lithology map and shows good agreement as with published lithology map. It has been observed that there was also some difference in the spatial distribution of lithological units between image results and published lithology map mainly due to the difference in the scale. The image based lithological map seems to provide much finer resolution as compared to published lithology map of 1:250000 scale.

5. Conclusion and future work

The study illustrated the effectiveness of ICA over PCA and MNF transform on ASTER SWIR data to discriminate the lithological units in the area. The proposed BC derived from ICA (R:IC2, G:IC3, B:IC1) has tremendous potential to discriminate various lithological units such as conglomerate, granite, gneiss, phyllites, mica schists, dolomitic and calcitic marble, synsedimentional volcanic, quartzite and pegmatites. The study has shown the effectiveness SWIR spectral bands of ASTER data in lithological mapping. The lithological map derived from image analysis could be further linked with the hydrothermal alteration zone and economic deposits such as lead-zinc and copper of the area. Thus, ASTER SWIR bands coupled with the advanced image enhancement technique like ICA is recommended as a rapid and cost effective tool for lithological discrimination and mapping in the hostile terrain of Rajasthan and other geological areas. The Future work could explore the development of lithological indices based on ICA transform for more accurate lithological identification and mapping. The Further work could also focused to explore these techniques on easily assessable multispectral imageries of Landsat 7 and 8 for regional lithological mapping.

Acknowledgement

The authors express their sincere thanks to anonymous reviewers for their constructive suggestions. The authors are grateful to ERDAC Japan and GSI for providing the ASTER data and District Resource Map of Udaipur and Rajsamand Area respectively to conduct this study.

References

1. Aboelkhair, H., Ninomiya, Y., Watanabe, Y., Sato, I. Processing and interpretation of ASTER TIR data for mapping of rare-metal-enriched albite granitoids in the Central Eastern Desert of Egypt. *Journal of African Earth Sciences* 2010; 58(1): 141-151.
2. Bedini, E. Mineral mapping in the Kap Simpson complex, central East Greenland, using HyMap and ASTER remote sensing data. *Advances in Space Research* 2011; 47(1): 60-73.
3. Clark, R.N. Spectroscopy of rocks, and minerals and principles of spectroscopy. In: Rencz, A.N., Ryerson, R.A. (Eds.), *Remote Sensing for the Earth Sciences*, Manual of Remote Sensing, 3rd ed. John Wiley & Sons 1999; New York, NY: 3–58.
4. Di Tommaso, I., Rubinstein, N. Hydrothermal alteration mapping using ASTER data in the Infiernillo porphyry deposit, Argentina. *Ore Geology Reviews* 2007; 32(1): 275-290.
5. Gabr, S., Ghulam, A., Kusky, T. Detecting areas of high-potential gold mineralization using ASTER data. *Ore Geology Reviews* 2010; 38(1): 59-69.
6. Gad, S., Kusky, T. Lithological mapping in the Eastern Desert of Egypt, the Barramiya area, using Landsat thematic mapper (TM). *Journal of African Earth Sciences* 2006; 44(2): 196-202.
7. Gad, S., Kusky, T. ASTER spectral ratioing for lithological mapping in the Arabian–Nubian shield, the Neoproterozoic Wadi Kid area, Sinai, Egypt. *Gondwana Research* 2007; 11(3): 326-335.
8. Galvão, L. S., Almeida-Filho, R., Vitorello, Í. Spectral discrimination of hydrothermally altered materials using ASTER short-wave infrared bands: Evaluation in a tropical savannah environment. *International Journal of Applied Earth Observation and Geoinformation* 2005; 7(2): 107-114.
9. Gomez, C., Delacourt, C., Allemand, P., Ledru, P., Wackerle, R. Using ASTER remote sensing data set for geological mapping, in Namibia. *Physics and Chemistry of the Earth 2005*; Parts A/B/C, 30(1): 97-108.
10. Gupta, S.N., Arora, Y.K., Mathur, R.K., Balluddin,I.Q., Prasad, B., Sahai, T.N., Sharma, S.B. Lithostatigraphic map of Aravalli region, South-eastern Rajasthan and northern Gujrat. Geological Survey of India 1981; Hyderabad.
11. Hewson, R.D., Cudahy, T.J., Mizujiko, S., Ueda, K., Mauger, A, L. Seamless geological map generation using ASTER in the Broken Hill-Curnmona province of Australia. *Remote Sensing of Environment* 2005; 99: 159-172.
12. Hosseinjani, M., Tangestani, M. H. Mapping alteration minerals using sub-pixel unmixing of ASTER data in the Sarduiyeh area, SE Kerman, Iran. *International Journal of Digital Earth* 2011; 4(6): 487-504.
13. Hyvarinen, A., E. Oja, Independent component analysis: algorithms and applications. Neural Networks 2000; vol. 13, no. 4-5: 411-430.
14. Kumar, C., Shetty, A., Raval, S., Champati Ray, P.K., Sharma, R. Sub-pixel mineral mapping using EO-1 Hyperion hyperspectral data. *International Archives of the Photogrammetry, Remote Sensing and Spatial Sciences* 2014: XL-8: 455-461. doi: 10.5194/isprsarchives-XL-8-455-2014.
15. Pour, A. B., Hashim, M. Identification of hydrothermal alteration minerals for exploring of porphyry copper deposit using ASTER data, SE Iran. *Journal of Asian Earth Sciences* 2011; 42(6): 1309-1323.
16. Pour, A. B., Hashim, M. Identifying areas of high economic-potential copper mineralization using ASTER data in the Urumieh–Dokhtar Volcanic Belt, Iran. *Advances in Space Research* 2012; 49(4): 753-769.
17. Qiu, F., Abdelsalam, M., Thakkar, P. Spectral analysis of ASTER data covering part of the Neoproterozoic Allaqi-Heiani suture, Southern Egypt. *Journal of African Earth Sciences* 2006; 44(2): 169-180
18. Rajendran, S., Al-Khirbash, S., Pracejus, B., Nasir, S., Al-Abri, A. H., Kusky, T. M., Ghulam, A. ASTER detection of chromite bearing mineralized zones in Semail Ophiolite Massifs of the northern Oman Mountains: Exploration strategy. *Ore Geology Reviews* 2012; 44: 121-135.
19. Rajendran, S., Nasir, S., Kusky, T. M., Ghulam, A., Gabr, S., El-Ghali, M. A. Detection of hydrothermal mineralized zones associated with listwaenites in Central Oman using ASTER data. *Ore Geology Reviews* 2013; 53: 470-488.
20. Richards, J.A. Remote Sensing Digital Image Analysis: An Introduction, Springer-Verlag Berlin, Germany 1999; p.240.
21. Rowan, L. C., Mars, J. C. Lithologic mapping in the Mountain Pass, California area using advanced spaceborne thermal emission and reflection radiometer (ASTER) data. *Remote Sensing of Environment* 2003; 84(3): 350-366.
22. Roy, A.B., Paliwal, B.S. Evolution of lower Proterozoic epicontinental deposits: stromatolite-bearing Aravalli rocks of Udaipur, Rajasthan, India. Precamb. Res 1981; 14: 49-74.
23. Roy, S.S., Malthottra, G., Mohanty, M. Geology of Rajasthan. Bangalore: Geology Society of India 1988.
24. Sabins, F. F. Remote sensing for mineral exploration. *Ore Geology Reviews* 1999; 14(3): 157-183.
25. Sinha-Roy, S., Mohanty, M., Guha, D.B. Dislocation Zone in Nathdwara-Khamour Area, Udaipur district, Rajasthan and its suignificance on the basement-cover relations in the Aravalli fold belt. Current Science 1993; 65(1): 68-72.
26. Tangestani, M. H., Jaffari, L., Vincent, R. K., Sridhar, B. M. Spectral characterization and ASTER-based lithological mapping of an ophiolite complex: A case study from Neyriz ophiolite, SW Iran. *Remote Sensing of Environment* 2011; 115(9): 2243-2254.
27. Van der Meer, F. D., Van der Werff, H. M., van Ruitenbeek, F. J., Hecker, C. A., Bakker, W. H., Noomen, M. F., & Woldai, T. Multi-and hyperspectral geologic remote sensing: A review. *International Journal of Applied Earth Observation and Geoinformation* 2012; 14(1): 112-128.
28. Zhang, X., Pazner, M., & Duke, N. Lithologic and mineral information extraction for gold exploration using ASTER data in the south Chocolate Mountains (California). *ISPRS Journal of Photogrammetry and Remote Sensing* 2007; 62(4): 271-282.

29. Zoheir, B., & Emam, A. Field and ASTER imagery data for the setting of gold mineralization in Western Allaqi–Heiani belt, Egypt: A case study from the Haimur deposit. *Journal of African Earth Sciences* 2014; 99: 150-164.